

Gaussian-Process-based Adaptive Tracking Control with Dynamic Active Learning for Autonomous Ground Vehicles

Kristóf Floch, Tamás Péni, and Roland Tóth

Abstract—This article proposes an active-learning-based adaptive trajectory tracking control method for autonomous ground vehicles to compensate for modeling errors and unmodeled dynamics. The nominal vehicle model is decoupled into lateral and longitudinal subsystems, which are augmented with on-line Gaussian Processes (GPs), using measurement data. The estimated mean functions of the GPs are used to construct a feedback compensator, which, together with an LPV state feedback controller designed for the nominal system, gives the adaptive control structure. To assist exploration of the dynamics, the paper proposes a new, dynamic active learning method to collect the most informative samples to accelerate the training process. To analyze the performance of the overall learning tool-chain provided controller, a novel iterative, counterexample-based algorithm is proposed for calculating the induced \mathcal{L}_2 gain between the reference trajectory and the tracking error. The analysis can be executed for a set of possible realizations of the to-be-controlled system, giving robust performance certificate of the learning method under variation of the vehicle dynamics. The efficiency of the proposed control approach is shown on a high-fidelity physics simulator and in real experiments using a 1/10 scale F1TENTH electric car.

I. INTRODUCTION

NOWADAYS, autonomous mobile robots, such as small-scale wheeled ground vehicles are becoming wide-spread in various industrial applications, hence, further improvement of autonomous maneuvering capabilities that can exploit the motion dynamics of these robots is a subject of scientific research. An essential prerequisite for reaching general utilization of these vehicles is the development of simple but effective control algorithms that can cope with unknown variations in the motion dynamics and can ensure high-performance maneuvering with formal guarantees of stability and performance.

The state-of-the-art trajectory tracking algorithms for ground vehicles are usually studied in the context of autonomous racing [1], utilizing both model-free [2], [3] and model-based [4], [5] approaches. While model-free methods have gained significant attention, in the context of autonomous vehicles, model-based solutions are still often favored due to safety concerns. The performance of model-based approaches

is dependent on the accuracy of the underlying model, therefore, precise identification of the motion dynamics is required. For this purpose, often first-principles-based models are used, but even after estimating the parameters of such models, unknown and hard-to-model dynamic effects that are specific to each vehicle often have significant effects on the behavior of the system. As a result, model uncertainties are inevitable and can lead to performance degradation in precise maneuvering in practice. To efficiently mitigate the effect of modeling uncertainties, adaptive algorithms have been extensively studied, which either estimate the parameters of the system dynamics, [6], or directly adapt the parameters of a control policy [7]. Furthermore, model augmentation, where a nominal vehicle model, typically based on first principles, is complemented with a learning component to capture the residual model mismatch, has been investigated. These methods usually utilize machine learning in terms of *artificial neural networks* (ANN) [8], or *Gaussian processes* (GP) [9] to capture the unknown model dynamics. GP augmentation has proven to be beneficial for a wide range of mobile robotic applications such as cars [10] quadcopters [11] and robotic arms [12], due to its high approximation capability and the uncertainty characterization of the estimates.

For GP-augmented models, *nonlinear model predictive control* (NMPC) algorithms are usually preferred [9]–[12]. However, due to the online optimization, real-time NMPCs require substantial computational resources compared to classical feedback methods, which are still applied in areas, where processing power is limited [5]. Therefore, this article proposes an effective GP-based compensation method with low computational complexity to adapt to modeling uncertainties.

Collecting measurement data for the training of the GPs in real-world scenarios is crucial for the effectiveness of the learning methods and it can be a time and energy-consuming task. Often, this step is overlooked in the literature. Furthermore, constraints of the specific environments (e.g. limited test areas, obstacles) and the motion dynamics of the vehicle make the data acquisition more challenging. Active learning methods have been a popular choice for the identification of unknown dynamics [13] and to refine GP models [14], [15] using their posterior distribution. However, existing methods assume that input-output training data can be easily collected, i.e., the function to be approximated can be evaluated at any value of its arguments. In our case, the inputs of the GP are the states of the motion dynamics. Therefore, to collect training data, the dynamic model has to be driven to the required

The authors are with the Systems and Control Laboratory, HUN-REN Inst. for Computer Science and Control, 1111 Budapest, Hungary (e-mails: kfloch@ethz.ch, peni@sztaki.hun-ren.hu, r.toth@tue.nl). R. Tóth is also affiliated with the Control Systems Group, Eindhoven University of Technology, 6512 Eindhoven, The Netherlands. This work was supported by the European Union within the Framework of the National Laboratory for Autonomous Systems under Grant RRF-2.3.1-21-2022-00002.

state configuration. To address this issue, we propose a novel dynamic active learning approach that takes into account the system dynamics and systematically designs experiments for data collection.

Lastly, providing performance guarantees is essential in autonomous robotic applications. Feedback algorithms for autonomous cars usually rely on decoupled and simplified dynamic models [16], [17] or are based on only kinematics [18], therefore, stability for the nonlinear closed-loop can not be guaranteed by design. However, computing stability guarantees for nonlinear systems is difficult, especially with learning components such as GPs or ANNs in the closed loop.

To summarize, the main expectations towards control algorithms for such vehicles are (a) adaptability to epistemic uncertainties, unknown dynamics and changing environmental conditions; (b) computationally efficient implementation; (c) guaranteed stability and performance. To address the presented challenges, our main contributions¹ are as follows:

- C1 We propose a computationally efficient GP-based adaptive trajectory tracking control architecture for car-like platforms, capable of handling large model mismatch.
- C2 We propose a recursive online sparse GP update technique, capable of jointly updating the hyperparameters and the inducing points of the GP.
- C3 We propose a novel active learning method for dynamic systems that utilizes the posterior distribution of the GPs to synthesize trajectories along which the learning components can be refined in a dynamic setting.
- C4 We provide a robust analysis approach in terms of the worst-case achievable \mathcal{L}_2 gain of the overall learning toolchain provided GP compensator under variations of the to-be-regulated vehicle dynamics.
- C5 We demonstrate the performance of the proposed adaptive methods in a high-fidelity simulator and in real experiments using the FITENTH platform [20].

The remainder of the paper is organized as follows. Sec. II provides an overview of GP regression and the proposed online recursive update method. It is followed by the problem formulation and the discussion of the baseline model in Sec. III. Sec. IV presents the proposed learning-based trajectory tracking algorithm, followed by dynamic active learning in Sec. V. Finally, the simulation study is presented in Sec. VII, while the experimental results are described in Sec. VIII.

II. GAUSSIAN PROCESS REGRESSION

Gaussian processes (GPs) have been a popular choice for model augmentation, see [9], [10], as they are efficient function estimators with direct characterization of the uncertainty of the estimate [21] and a manageable computational load compared to Bayesian neural networks. Compared to most of the other learning approaches such as ANNs, the uncertainty of the approximation can be employed for designing controllers that guarantee robust performance of closed-loop despite the uncertainty of the model of the underlying behavior of the

¹A preliminary version of the proposed control architecture has been published in [19]. This article extends [19] by the online training of the GPs, the experiment design by active learning, extended performance guarantees, and real-world experimental evaluation.

plant [22]. Next, we give a brief overview of GP-based modeling and techniques that enable real-time implementation.

A. Gaussian Processes

To estimate a scalar unknown function $f : \mathbb{R}^{n_x} \rightarrow \mathbb{R}$ with a GP, let $X^N = [x_1^\top \cdots x_N^\top] \in \mathbb{R}^{N \times n_x}$ denote the collection of N number of input values and let $Y^N = [y_1 \cdots y_N]^\top \in \mathbb{R}^N$ be the corresponding noisy output measurements, forming the data set $\mathcal{D}^N = \{X^N, Y^N\}$, generated by the following model:

$$y_i = f(x_i) + \epsilon_i, \quad i \in \mathbb{I}_1^N, \quad (1)$$

where $\epsilon_i \sim \mathcal{N}(0, \sigma_\epsilon^2)$ is an i.i.d. Gaussian noise and $\mathbb{I}_{\tau_1}^{\tau_2} = \{i \in \mathbb{Z} \mid \tau_1 \leq i \leq \tau_2\}$. The core idea of GP-based estimation of f is to consider that candidate estimates g belong to a GP, seen as a prior distribution. Then, using \mathcal{D}_N and this prior, a predictive GP distribution of g is computed that provides an estimate of f in terms of its mean and describes the uncertainty of this estimate by its variance.

In terms of definition, a scalar-valued *Gaussian Process* \mathcal{GP} assigns to every point $x \in \mathbb{R}^{n_x}$ a random variable $\mathcal{GP}(x)$, such that, for any finite set $\{x_i\}_{i=1}^N \subset \mathbb{R}^{n_x}$, the joint probability distribution of $\mathcal{GP}(x_1), \dots, \mathcal{GP}(x_N)$ is Gaussian. Due to this property, $g \sim \mathcal{GP}(m, \kappa)$ is fully determined by its mean m and covariance κ expressed as

$$m(x) = \mathbb{E}[g(x)], \quad (2a)$$

$$\kappa(x, \tilde{x}) = \mathbb{E}[(g(x) - m(x))(g(\tilde{x}) - m(\tilde{x}))], \quad (2b)$$

where $x, \tilde{x} \in \mathbb{R}^{n_x}$ and \mathbb{E} is the expectation. This distribution describes our prior belief of the function space in which estimate of the the unknown function f is searched for. In the remainder of the paper, we assume w.l.o.g. that the prior mean is zero ($m(x) = 0$) and covariance of the distribution is characterized with a *squared exponential* (SE) kernel, a common choice for estimation of smooth functions:

$$\kappa_{\text{SE}}(x, \tilde{x}) = \sigma_f^2 \exp\left(-\frac{1}{2}(x - \tilde{x})^\top \Lambda^{-1}(x - \tilde{x})\right), \quad (3)$$

where $\sigma_f \in \mathbb{R}$ is a scaling factor and $\Lambda \in \mathbb{R}^{n_x \times n_x}$ is a positive definite and symmetric matrix that determines the smoothness of the candidate functions. The parameters of the considered kernel function, i.e., σ_f , Λ and σ_ϵ in (1) are the so-called hyperparameters of the prior distribution and they are collected in the vector $\theta \in \mathbb{R}^{n_\theta}$. Note that other kernels can also be considered as it is discussed in [21].

Based on \mathcal{D}^N and the prior $g \sim \mathcal{GP}(m, \kappa)$,

$$p(Y^N | X^N, \theta) = \mathcal{N}(0, K_{NN} + I\sigma_\epsilon^2) \quad (4)$$

is the probability density function of the Y^N outputs seen as random variables conditioned on X^N and θ , where $[K_{NN}]_{i,j} = \kappa(x_i, x_j)$, $i, j \in \mathbb{I}_1^N$. Simple derivation leads to that the predictive distribution for $g(x_*)$ at test point x_* is the posterior $p(g(x_*) | \mathcal{D}^N, x_*) = \mathcal{N}(\mu(x_*), \Sigma(x_*))$, with

$$\mu(x_*) = K_N^\top(x_*)(K_{NN} + \sigma_\epsilon^2 I)^{-1} Y^N, \quad (5a)$$

$$\Sigma(x_*) = \kappa(x_*, x_*) - K_N^\top(x_*)(K_{NN} + \sigma_\epsilon^2 I)^{-1} K_N(x_*), \quad (5b)$$

where $[K_N(x_*)]_i = \kappa(x_i, x_*)$, $i \in \mathbb{I}_1^N$. Eq. (5a) characterizes the mean as the approximation of the unknown function f

and (5b) is the variance, which gives the uncertainty of the approximation.

Tuning the GP estimate, i.e., shaping the resulting posterior distribution, can be achieved by adjusting the previously introduced hyperparameters. An efficient approach for this follows via maximizing the marginal likelihood w.r.t. the hyperparameters, i.e.,

$$\theta^* = \arg \max_{\theta} \{\log p(Y^N | X^N, \theta)\}, \quad (6)$$

where

$$\begin{aligned} \log p(Y^N | X^N, \theta) &= -\frac{N}{2} \log(2\pi) \\ &- \frac{1}{2} Y^{N\top} (K_{NN} + \sigma_\epsilon^2 I)^{-1} Y^N - \frac{1}{2} \log \det(K_{NN} + \sigma_\epsilon^2 I). \end{aligned} \quad (7)$$

Commonly, (7) is solved via standard gradient-based optimization such as conjugate gradient descent, providing an efficient way to optimize the hyperparameters.

As every training point is required for making predictions, the computational complexity of (5a) is $\mathcal{O}(N)$ and of (5b) is $\mathcal{O}(N^2)$, while the training is $\mathcal{O}(N^3)$ due to the evaluation (7). Therefore, in case of large training datasets, the real-time implementation of GP estimators is computationally expensive.

B. Sparse Gaussian Processes

One way to tackle the computational limitation of GP regression is to use *sparse* GPs (SGPs), where the number of data points used in the evaluation is limited to a fixed number. The goal of the SGP is to create a virtual dataset (often referred to as inducing points) defined as $\mathcal{D}^M = \{X^M, Y^M\}$, where $X^M = [\hat{x}_1^\top \cdots \hat{x}_M^\top] \in \mathbb{R}^{M \times n_x}$ and $Y^M = [\hat{y}_1 \cdots \hat{y}_M] \in \mathbb{R}^M$ such that the Kullback-Leiber (KL) divergence between the posteriori distribution obtained from \mathcal{D}^M and the original distribution based on \mathcal{D}^N is minimal, while $M \ll N$.

To find the proper \mathcal{D}^M set, we utilize the *variational free energy* (VFE) approach [23] in which a variational method is used that jointly selects the X^M and the hyperparameters.

In the VFE approach, the objective can be expressed as

$$\begin{aligned} \mathcal{L}(\mathcal{D}^N, X^M, \theta) &= \frac{N}{2} \log(2\pi) + \frac{1}{2} Y^\top (W_{NN} + \sigma_\epsilon^2 I_N) Y \\ &+ \frac{1}{2} \log \det(W_{NN} + \sigma_\epsilon^2 I_N) + \frac{1}{2} \text{tr}(K_{NN} - W_{NN}) \end{aligned} \quad (8)$$

where $W_{NN} = K_{NM} K_{MM}^{-1} K_{MN}$ with $[K_{MN}]_{i,j} = \kappa(\hat{x}_i, x_j)$, $i \in \mathbb{I}_1^M$, $j \in \mathbb{I}_1^N$, which is the covariance matrix between the pseudo inputs and all training inputs, $[K_{MM}]_{i,j}$, $i, j \in \mathbb{I}_1^M$ is the covariance of the pseudo inputs. By maximizing (8), the hyperparameters of the GP and the pseudo inputs can be jointly obtained, i.e.

$$(\theta^*, X^{M^*}) = \arg \max_{\theta, X^M} \mathcal{L}(\mathcal{D}^N, X^M, \theta), \quad (9)$$

which is a nonlinear optimization that can be reliably solved. Furthermore, note that the pseudo outputs do not appear in the optimization, as they are fully represented by the approximative GP and the pseudo-inputs.

After the training, the resulting posterior distribution at an arbitrary test point x_* is $\mathcal{N}(\mu_p(x_*), \Sigma_p(x_*))$, with

$$\mu_p(x_*) = K_M^\top(x_*) Q_{MM} K_{MN} \sigma_\epsilon^{-2} Y^N, \quad (10a)$$

$$\Sigma_p(x_*) = \kappa(x_*, x_*) - W_{MM}(x_*) + K_M^\top(x_*) K_{MM}^{-1} K_M(x_*), \quad (10b)$$

where $[K_M(x_*)]_i = \kappa(x_i, x_*)$, $i \in \mathbb{I}_1^M$ and $W_{MM}(x_*) = K_M^\top(x_*) K_{MM}^{-1} K_M(x_*)$, which corresponds to a Nyström projection of the original GP to the pseudo inputs X^M . This formulation reduces the $\mathcal{O}(N^3)$ computational complexity of the evaluation of the mean to $\mathcal{O}(M)$ and the training to $\mathcal{O}(NM^2)$. In the following sections, SGPs will be utilized as the learning component of the proposed adaptive control approach.

C. Online Learning and Update for SGPs

The VFE method is constructed for offline training, i.e., it requires the complete training set to be available. For adaptive control, online training is more suitable as it updates the model during operation using the latest measurement data. For training GPs online, various algorithms such as the *recursive least squares* GP (RLS-GP) [11] or the *dynamic sparse* GP (DS-GP) [10] are available. This article proposes a *recursive gradient-based* (RGB) optimization scheme for SGPs utilizing the VFE method outlined in Sec. II-B. Compared to the previously introduced techniques that either update the approximate posterior distribution (RLS-GP) or the inducing points (DS-GP), this approach jointly updates both the hyperparameters and the inducing points of the GP based on the incoming new information, which to the authors knowledge has not been applied before.

First, we assume that the SGP has been trained offline on the initial dataset \mathcal{D}^N , yielding the optimal values for θ hyperparameters and X^M inducing points that correspond to Y^M virtual outputs. As outlined before, the core idea of sparse GP estimation is that the virtual D^M dataset is obtained such that its distribution approximates the original D^N set with considerably fewer data points. Therefore, in future predictions, we can rely only on the D^M set, as it represents the information content of D^N .

Let the one incoming batch of input-output data at time step k be denoted as $\mathcal{D}_k^Z = \{X_k^Z, Y_k^Z\}$, where $X_k^Z = [x_1^\top \cdots x_Z^\top] \in \mathbb{R}^{Z \times n_x}$, $Y_k^Z = [y_1 \cdots y_Z] \in \mathbb{R}^Z$ and Z is the batch size. Then, after receiving one batch of new training data at time k , we can combine the previously obtained pseudo dataset and the new batch to define a new training dataset as $\hat{\mathcal{D}}_k = \mathcal{D}_{k-1}^M \cup \mathcal{D}_k^Z$, where $\mathcal{D}_0^M = \mathcal{D}^M$. Note that with this formulation, $\hat{\mathcal{D}}_k$ both contains information from the pre-trained GP and innovation from the update batch. By substituting this combined dataset into the VFE cost (8), we can perform n_α steps of gradient descent to collectively update the hyperparameters of the GP and the inducing points, i.e.

$$\begin{bmatrix} X_i^M \\ \theta_i \end{bmatrix} = \begin{bmatrix} X_{i-1}^M \\ \theta_{i-1} \end{bmatrix} - \alpha \frac{\partial \mathcal{L}}{\partial \begin{bmatrix} X_i^M \\ \theta_i \end{bmatrix}} (\hat{\mathcal{D}}_k, X_i^M, \theta_i), \quad (11)$$

where α is the learning rate and $i \in \mathbb{I}_1^{n_\alpha}$. Note that the evaluation of (11) has the computational complexity of $\mathcal{O}((M +$

Algorithm 1 Optimization-based batch update.

- 1: **input:** \mathcal{D}_{k-1}^M original pseudo dataset, θ_{k-1} hyperparameters, \mathcal{D}_k^Z update batch, α learning rate, n_α number of gradient steps (retraining iterations)
 - 2: $\hat{\mathcal{D}}_k \leftarrow \mathcal{D}_{k-1}^M \cup \mathcal{D}_k^Z$
 - 3: $\hat{X}_0^M \leftarrow X_k^M$
 - 4: $\hat{\theta}_0 \leftarrow \theta_k$
 - 5: **for** $i \leftarrow 1$ **to** n_α **do**
 - 6: Calculate \hat{X}_i^M and $\hat{\theta}_i$ using (11) with $\hat{\mathcal{D}}_k$, \hat{X}_{i-1}^M , $\hat{\theta}_{i-1}$
 - 7: **end for**
 - 8: $\mathcal{D}_k^M \leftarrow \hat{\mathcal{D}}_{n_\alpha}$
 - 9: $\theta_k \leftarrow \hat{\theta}_{n_\alpha}$
 - 10: **return** \mathcal{D}_k^M and θ_k
-

$Z)M^2$), therefore, gradient descent can be executed multiple times online in one update iteration. Furthermore, using the augmented training dataset $\hat{\mathcal{D}}_k$ is beneficial as it incorporates both the previously learned knowledge from \mathcal{D}_{k-1}^M and the new information contained in \mathcal{D}_k^Z . The RBG algorithm is outlined in Alg. 1 and has three important parameters: the size of the pseudo dataset M and the update batch size Z and n_α number of retrain iterations.

III. VEHICLE MODEL & TRAJECTORY TRACKING

A. Trajectory Tracking

The primary aim of this paper is to provide precise tracking of reference trajectories in the presence of modeling uncertainties. To outline the trajectory tracking problem, we first define the reference trajectories. The path is expressed as a two-dimensional spline curve $\psi(s^{\text{ref}}(t))$, defined by the coordinate functions $(x(s^{\text{ref}}(t)), y(s^{\text{ref}}(t)))$, where s^{ref} is a time domain signal defined as $s^{\text{ref}} : \mathbb{R} \rightarrow [0, L]$. The arc length of the full path is denoted as L , hence $s^{\text{ref}}(t)$ describes the desired vehicle position along the path at time t . Both $x(s^{\text{ref}}(t))$, and $y(s^{\text{ref}}(t))$ are monotonic in $s^{\text{ref}}(t)$, furthermore $(x(0), y(0))$ and $(x(L), y(L))$ assign the endpoints of the curve. The speed reference $v^{\text{ref}}(s^{\text{ref}}(t)) = v^{\text{ref}}(t)$ along the trajectory is also given. These types of reference motion trajectories can be obtained by regular path planning algorithms.

B. Baseline Vehicle Model

The baseline vehicle model relies on a dynamic single-track representation, which has been commonly used for describing the behavior of small-scale car-like vehicles, see [4], [24]. The modeling concept is depicted in Fig. 1 and the resulting model is described as

$$\dot{x} = v_\xi \cos(\varphi) - v_\eta \sin(\varphi), \quad (12a)$$

$$\dot{y} = v_\xi \sin(\varphi) + v_\eta \cos(\varphi), \quad (12b)$$

$$\dot{\varphi} = \omega, \quad (12c)$$

$$\dot{v}_\xi = \frac{1}{m} (F_\xi + F_\xi \cos(\delta) - F_{f,\eta} \sin(\delta) + mv_\eta \omega), \quad (12d)$$

$$\dot{v}_\eta = \frac{1}{m} (F_{r,\eta} + F_\xi \sin(\delta) + F_{f,\eta} \cos(\delta) - mv_\xi \omega), \quad (12e)$$

$$\dot{\omega} = \frac{1}{I_z} (F_{f,\eta} l_f \cos(\delta) + F_{f,\xi} l_f \sin(\delta) - F_{r,\eta} l_r), \quad (12f)$$

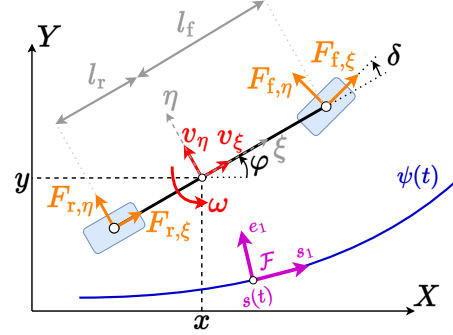


Fig. 1. Single-track vehicle model and reference trajectory.

where (x, y) is the position and φ is the orientation of the vehicle in the global coordinate frame. The states v_ξ and v_η denote the longitudinal and lateral velocity of the vehicle in a body fixed frame and ω is the yaw rate. The parameters of the model are the distance of the front and rear axis from the center of mass, denoted as l_f and l_r , the mass of the vehicle m and the inertia along the vertical axis I_z .

The longitudinal tire force F_ξ is determined by a drivetrain model, which assumes a first-order connection between the motor input and the velocity of the vehicle. This modeling technique has been successfully utilized previously in [24] and [4] for electric vehicles, hence, we adopted the following variant:

$$F_\xi = C_{m1}d - C_{m2}v_\xi - C_{m3}, \quad (13)$$

where C_{m1} , C_{m2} , C_{m3} are lumped drivetrain parameters and $d \in [0, 1]$ is the motor input. Lastly, the lateral tire forces are often calculated using a simplified linear tire model as

$$F_{r,\eta} = C_r \arctan((-v_\eta + l_r \omega)/v_\xi), \quad (14a)$$

$$F_{f,\eta} = C_f \arctan(\delta - (v_\eta + l_f \omega)/v_\xi), \quad (14b)$$

where C_f and C_r are the cornering stiffness of the front and rear tire respectively. Finally, the control inputs of the vehicle are the steering angle δ and the motor input d , which a controller can directly actuate.

Using the trajectory description of Sec. III-A, we can transform (12) into a curvilinear coordinate frame (depicted in Fig. 1 as \mathcal{F}) that is parameterized by the position along the reference path [24]:

$$\dot{s} = (v_\xi \cos(\theta_e) - v_\eta \sin(\theta_e))/(1 - c(s)e_s), \quad (15a)$$

$$\dot{e}_s = v_\xi \sin(\theta_e) + v_\eta \cos(\theta_e), \quad (15b)$$

$$\dot{\theta}_e = \omega - c(s)\dot{s}, \quad (15c)$$

where the newly introduced states are the position s along the path, the lateral deviation e_s and the heading error θ_e , while the lateral (v_η), longitudinal (v_ξ) and angular velocities (ω) are the same as in (12). Furthermore, $c(s)$ describes the curvature of the reference path at s .

The main advantage of this model is that the tracking errors explicitly appear in (15), which is beneficial for the control design. Furthermore, due to the physics-inspired model description, all the states can be easily determined from measurements, which allows the design of a full state-feedback controller for the vehicle.

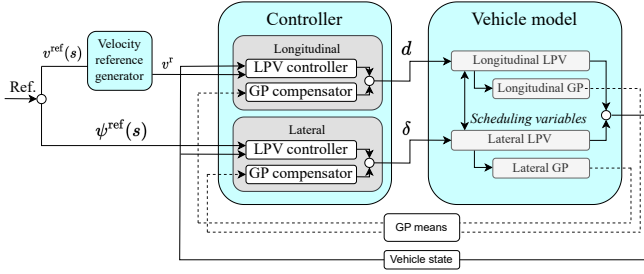


Fig. 2. Proposed control architecture for trajectory tracking.

IV. GP-BASED ADAPTIVE CONTROL

A. Control Architecture

Based on the trajectory tracking model (15), we propose a computationally efficient adaptive feedback control algorithm. For this, we decouple the nonlinear vehicle dynamics into two subsystems, corresponding to the longitudinal and lateral motion of the vehicle. Then, to adapt to modeling uncertainties and external disturbances, we augment each subsystem with a GP-based compensator to eliminate the effect of structural model bias. Finally, based on the remaining nominal model, we synthesize LQ state-feedback controllers to track the given reference. The overall architecture is depicted in Fig. 2.

B. Decoupling

We decouple (15) into lateral and longitudinal subsystems for individual control design. The longitudinal controller is responsible for tracking the reference velocity and position along the path and the lateral controller is used for path tracking.

From (15), the **longitudinal model** becomes

$$\dot{s} = (v_\xi \cos(\theta_e) - v_\eta \sin(\theta_e)) / (1 - c(s)e_s), \quad (16a)$$

$$\dot{v}_\xi = \frac{1}{m} ((1 + \cos(\delta))(C_{m1}d - C_{m2}v_\xi - C_{m3}) - F_{f,\eta} \sin(\delta) + mv_\eta\omega), \quad (16b)$$

where the state vector $x_{1o} = [s \ v_\xi]^\top$ is the position along the path and the longitudinal velocity, while d is the actuated control input. Furthermore, the heading error θ_e , lateral deviation e_s , lateral velocity v_η , steering angle δ and $F_{f,\eta}$ are considered as external varying parameters depending on the lateral subsystem. The reference input of the system is $x_{1o}^{\text{ref}} = [s^{\text{ref}} \ v^{\text{ref}}]^\top$ defined by the trajectory. To simplify the control design and analysis, we separate the position and velocity states by introducing a virtual velocity generator that provides a position-adjusted virtual reference velocity as $v^r = v^{\text{ref}} - k_v(s - s^{\text{ref}})$. This results in the modified control objective $v_\xi \rightarrow v^r$, while the model dimensions are reduced, as only the dynamics of v_ξ are needed to be considered. Therefore, the longitudinal behavior can be expressed as:

$$\underbrace{\dot{v}_\xi}_{\dot{x}_{1o}} = \underbrace{\frac{-C_{m2}(1 + \cos(\delta))}{m}}_{A_{1o}(\delta)} v_\xi + \underbrace{\frac{C_{m1}(1 + \cos(\delta))}{m}}_{B_{1o}(\delta)} d + \underbrace{\frac{-C_{m3}(1 + \cos(\delta))}{m}}_{w_0} + \underbrace{\frac{-F_{f,\eta} \sin(\delta)}{m}}_{w_1} + v_\eta\omega \quad (17)$$

where $A_{1o}(\delta)$ and $B_{1o}(\delta)$ can be considered as parameter-varying state-transition and input matrices with steering angle δ as a scheduling variable, resulting in a *linear parameter-varying* (LPV) embedding [25]. Here, w_0 is a nonlinearity introduced by the dry friction of the drivetrain and w_1 lumps together the effects of the lateral subsystem.

From (15), the **lateral** behavior of the vehicle is described as

$$\dot{e}_s = v_\xi \sin(\theta_e) + v_\eta \cos(\theta_e), \quad (18a)$$

$$\dot{\theta}_e = \omega - c(s)\dot{s}, \quad (18b)$$

$$\dot{v}_\eta = \frac{1}{m} (F_{r,\eta} + F_\xi \sin(\delta) + F_{f,\eta} \cos(\delta) - mv_\xi\omega), \quad (18c)$$

$$\dot{\omega} = \frac{1}{I_z} (F_{f,\eta} l_f \cos(\delta) + F_{f,\xi} l_f \sin(\delta) - F_{r,\eta} l_r), \quad (18d)$$

where the state vector $x_{1a} = [e_s \ \theta_e \ v_\eta \ \omega]^\top$ consists of the lateral error e_s , heading error θ_e , lateral velocity v_η and yaw rate ω , while v_ξ is a scheduling variable. The input is steering angle δ . To simplify the model, we first substitute the lateral tire models into (18), use small angle approximations ($\sin(\alpha) \approx \alpha$, $\cos(\alpha) \approx 1$), neglect the longitudinal tire force ($F_\xi \approx 0$) and approximate the velocity along the path as $\dot{s} \approx v_\xi$ which leads to the model:

$$\begin{bmatrix} \dot{e}_s \\ \dot{v}_\eta \\ \dot{\theta}_e \\ \dot{\omega} \end{bmatrix} = \begin{bmatrix} 0 & 1 & v_\xi & 0 \\ 0 & A_{vv} & 0 & A_{v\omega} \\ 0 & 0 & 0 & 1 \\ 0 & A_{\omega v} & 0 & A_{\omega\omega} \end{bmatrix} \begin{bmatrix} e_s \\ v_\eta \\ \theta_e \\ \omega \end{bmatrix} + \begin{bmatrix} 0 \\ \frac{C_f}{m} \\ 0 \\ \frac{l_f C_f}{I_z} \end{bmatrix} \delta + \begin{bmatrix} 0 \\ 0 \\ v_\xi \\ 0 \end{bmatrix} c(s), \quad (19)$$

where $A_{vv} = -\frac{C_f + C_r}{mv_\xi}$, $A_{v\omega} = -v_\xi - \frac{l_f C_f - l_r C_r}{mv_\xi}$, $A_{\omega v} = \frac{l_r C_r - l_f C_f}{I_z v_\xi}$, $A_{\omega\omega} = -\frac{l_f^2 C_f + l_r^2 C_r}{I_z v_\xi}$. Note, that in (19) the path curvature is regarded as an external disturbance. Further simplification can be achieved by expressing the lateral model only in terms of the error variables and their derivatives, i.e., by introducing $\ddot{e}_s = \dot{v}_\eta + v_\xi \dot{\theta}_e$. As discussed in [26], regulating both the heading and the lateral error to the origin yields poor tracking performance, as the two quantities cannot be simultaneously zero along the path if we assume perfect tracking. Therefore, we separate the lateral error and the heading dynamics. We use the lateral error dynamics for feedback control design and only regulate the heading error with a feedforward, similar to the Stanley controller [27]. Furthermore, we also introduce the integral of the lateral error, i.e., $q(t) = \int_0^t e_s(\tau) d\tau$ as a new state to assure asymptotic convergence of e_s without offset. The final control-oriented lateral model can be expressed as

$$\underbrace{\begin{bmatrix} \dot{q} \\ \dot{e}_s \\ \ddot{e}_s \end{bmatrix}}_{\dot{x}_{1a}} = \underbrace{\begin{bmatrix} 0 & 1 & 0 \\ 0 & 0 & 1 \\ 0 & 0 & -\frac{C_f + C_r}{mv_\xi} \end{bmatrix}}_{A_{1a}(v_\xi)} \underbrace{\begin{bmatrix} q \\ e_s \\ \dot{e}_s \end{bmatrix}}_{x_{1a}} + \underbrace{\begin{bmatrix} 0 \\ 0 \\ \frac{C_f}{m} \end{bmatrix}}_{B_{1a}} \delta + \underbrace{\begin{bmatrix} 0 \\ 0 \\ \frac{l_r C_r - l_f C_f}{m} - 1 \end{bmatrix}}_{B_c} c(s) + \underbrace{\begin{bmatrix} 0 & 0 \\ 0 & 0 \\ \frac{C_r + C_f}{m} & -\frac{l_f^2 C_f + l_r^2 C_r}{I_z v_\xi} \end{bmatrix}}_{B_2(v_\xi)} \underbrace{\begin{bmatrix} \theta_e \\ \dot{\theta}_e \end{bmatrix}}_{w_2}, \quad (20)$$

where the state vector $\chi_{1a} = [q \ e_s \ \dot{e}_s]^\top$ now only contains the lateral error, its integral and derivative, while $A_{1a}(v_\xi)$ is the parameter varying state-transition matrix with scheduling signal v_ξ and B_{1a} is the input matrix. Moreover, w_c is the path curvature and w_2 is used to lump together the unmodeled path and heading dynamics.

C. GP-based Model Augmentation

Note that we have made simplifications during the derivation of (17) and (20). Furthermore, due to modeling uncertainties, the model mismatch between the control-oriented model and the true vehicle can significantly decrease the tracking performance. Therefore, to capture this model mismatch, we augment the nominal models (17) and (20) with GPs:

$$\dot{\chi}_{1a} = A_{1a}(v_\xi)\chi_{1a} + B_{1a}\delta + B_c w_c + B_{\mathcal{GP}}\mathcal{GP}_{1a}(z), \quad (21a)$$

$$\dot{\chi}_{1o} = A_{1o}(\delta)\chi_{1o} + B_{1o}(\delta) + w_0 + \mathcal{GP}_{1o}(z), \quad (21b)$$

where $\mathcal{GP}_{1o}(z)$ and $\mathcal{GP}_{1a}(z)$ denote the GPs linked to the lateral and longitudinal subsystems, respectively. Based on the structure of the nominal path following model (15), we can observe that the first three equations only capture kinematic relationships. Therefore, we assume that modeling uncertainties only affect the velocity states v_ξ , v_η , ω , as proposed in [10]. Furthermore, we can also note that $B_{\mathcal{GP}} = [0 \ 0 \ 1]^\top$ as uncertain dynamic effects only influence \dot{e}_s . Observing the original vehicle model (12), we can also note that any change in the environmental conditions affects the dynamics through the acting wheel forces. As these models depend on the velocity states, we choose these variables to construct the GPs. Therefore, the inputs for both the lateral and the longitudinal GPs are $z = [v_\xi \ v_\eta \ \omega]^\top$.

As we previously assumed that all the vehicle states are available, training inputs can be collected from the logged measurement data of driving experiments with the vehicle. By numerical differentiation, we can obtain the state derivatives and the outputs for the GPs can be expressed from (21) to generate the training dataset. Note that process noise effects are handled through the GP estimation process, corresponding to a NARX setting. Colored process noise scenarios can be either handled by appropriate parametrization of the noise covariance/kernel [21] or in case of more elaborate noise settings, using instrumental variables for the mean function estimation [28]. Furthermore, because of the large training dataset, utilization of SGPs is necessary to reduce the computation complexity of both the estimation and the online evaluation.

D. Adaptive Control Design

We propose an adaptive control scheme, which consists of two main components: an adaptive compensator term that accounts for model mismatch, and a nominal offline-designed LPV controller that provides accurate tracking when the model parameters are reliably known.

With the compensator terms, the means of the GPs μ_{1o} and μ_{1a} are cancelled by introducing the following compensatory terms:

$$d_{\mathcal{GP}} = 1/B_{1o}(\delta)\mu_{1o}(z), \quad (22a)$$

$$\delta_{\mathcal{GP}} = B_{1a}^\dagger B_{\mathcal{GP}}\mu_{1a}(z). \quad (22b)$$

The adaptivity of (22) comes from the recursive estimation and compensation with the GPs. Furthermore, the posterior variance characterizing the uncertainty of the GP approximation is utilized to systematically collect informative training data and thus improve the sample efficiency of learning [15].

Assuming that (22) can eliminate the model mismatch, we stabilize the subsystems by the following control laws:

$$\delta_{\text{nom}} = K_{1a}(v_\xi)\chi_{1a} - \theta_e - B_{1a}^\dagger B_c w_c, \quad (23a)$$

$$d_{\text{nom}} = K_{1o}(\delta)(v_\xi - v^r) + 1/B_{1o}(\delta)A_{1o}(\delta)v^r - 1/B_{1o}(\delta)w_0, \quad (23b)$$

where $K_{1a}(v_\xi)$ and $K_{1o}(\delta)$ are parameter-dependent gain matrices and the additional terms are used to achieve reference tracking and to cancel out known disturbances. The feedback matrices are obtained using the nominal subsystems (17) and (20) with the LPV-LQR synthesis proposed in [29]. In the latter sections of this work, we refer to (23) as the *nominal* part of the controller and (23) and (22) combined as the *adaptive* part of the controller.

Consider an LPV system in the general form as $\dot{X} = A(\rho)X + B(\rho)u$. The optimal parameter dependent state feedback matrix $K(\rho)$ that minimizes the quadratic cost $J_{LQ} = \int_0^\infty \chi^\top(t)Q\chi(t) + u^\top(t)Ru(t) dt$ with $Q \in \mathbb{R}^{n_x \times n_x}$ and $R \in \mathbb{R}^{n_u \times n_u}$ can be obtained by solving the convex optimization problem:

$$\max_{K, X, Y} \text{trace}(X), \quad (24a)$$

$$\text{s.t. } X \succ 0, \quad (24b)$$

$$M(X, Y, Q, R, \rho) \succ 0 \quad \forall \rho \in \mathbb{G}, \quad (24c)$$

where $X \in \mathbb{R}^{n_x \times n_x}$, and the *linear matrix inequality* (LMI) constraint $M(X, Y, Q, R, \rho)$ is defined as

$$\begin{bmatrix} -\text{He}(A(\rho)X + B(\rho)Y(\rho)) & (QX + \mathcal{R}Y(\rho))^\top \\ (QX + \mathcal{R}Y(\rho)) & I \end{bmatrix} \quad (25)$$

where the gain matrices of the quadratic cost are encoded in $Q = [Q^{\frac{1}{2}} \ 0]^\top$ and $\mathcal{R} = [0 \ R^{\frac{1}{2}}]^\top$ and $\text{He}(X) = X^\top + X$. Furthermore, $Y(\rho) \in \mathbb{R}^{n_u \times n_x}$ is parameterized as follows:

$$Y(\rho) = Y_0 + \rho Y_1 + \rho^2 Y_2 + \dots + \rho^n Y_n \quad (26)$$

and $\mathbb{G} \subset \Gamma$ is a discrete grid of the scheduling region, used to relax the infinite number of LMI constraints. After solving (24), the parameter-dependent feedback matrix is obtained as $K(\rho) = Y(\rho)X^{-1}$. The parameter-dependent state-feedback gains K_{1o} and K_{1a} for the longitudinal and lateral subsystems have been obtained using the outlined LPV-LQR synthesis with a priori fixed weighting matrices Q_{1o} , Q_{1a} , R_{1o} , R_{1a} .

V. DYNAMIC ACTIVE-LEARNING FOR EXPERIMENT DESIGN

A. Problem Statement

The main objective of the experiment design is to collect data points where the approximation of the GP is less reliable, i.e., where the GP needs the most improvement. This problem has been addressed by active learning methods [14], [15], which use the variance of the posterior distribution of the GPs to find new training points. However, these methods cannot

be applied in dynamic scenarios such as ours as the input of the GPs corresponds to state variables which means that the vehicle has to be navigated to a certain state configuration for the evaluation. Therefore systematic trajectory planning is required, taking into account the system dynamics. Therefore, we propose an experiment design that incorporates the system dynamics into active learning and directly synthesizes trajectories to explore regions where the variance of the posterior distribution of the GPs is high. Then, completing the training dataset with new data collected along the resulting trajectory, the GPs can be retrained. In the next sections, we consider our specific scenario, where the inputs of the lateral and longitudinal GPs are the velocity states ($z = [v_\xi \ v_\eta \ \omega]^\top$) of the nonlinear model (12). Given baseline GP models, we utilize their posterior distribution to formulate a numerical optimization problem to obtain trajectories for the refinement of the approximation.

B. Trajectory Parameterization

The spatial trajectories can be easily parameterized with splines, see Sec. III. However, if all spline parameters are considered free variables, the complexity of solving a planning task increases significantly, and imposing shape constraints is difficult. Therefore, we adopt a modified version of the parameterization in [30]. Let an initial trajectory be denoted as $\mathcal{T}_0 = \{\psi_0(s), v_0(s)\}$, where $\psi_0(s)$ is a two dimensional arc-length parameterized spline curve and $v_0(s)$ is the corresponding speed profile. For ψ_0 , we define n number of nodes $\{s_i\}_{i=1}^n$ along this initial path which can be chosen based on various strategies, e.g. equidistantly. These are depicted with green dots in Fig. 3. Then, we define new waypoints by moving the node by w_i along a line perpendicular to the \mathcal{T}_0 trajectory, where $w_i \in [-w_b/2, w_b/2]$ interval. These waypoints are depicted as red crosses. Then, using 2D spline interpolation on the waypoints, we can obtain the path $\psi_W(s)$, which is parameterized by $W = [w_1, \dots, w_n]$ and the initial trajectory ψ_0 , as depicted in Fig. 3.

A similar approach can be used for the speed profiles. We consider a generic initial speed profile $v_0(s)$. Then, we define n nodes along s like in the spatial coordinates, depicted in Fig. 3. By perturbing the velocity profile by $\tilde{v}_i \in [v_{\min} - v_0(s_i), v_{\max} - v_0(s_i)]$, $i \in \mathbb{I}_1^n$ at each node, we can first define profile points, then, by using spline interpolation, obtain a new speed profile $v_V(s)$ directly parameterized by $V = [v_0(s_1) + \tilde{v}_1 \dots v_0(s_n) + \tilde{v}_n]$. The main benefit of using this parameterization is that a trajectory can be described by $2n$ number of parameters, which is a significant reduction compared to the full spline parameterization. Furthermore, all parameters have clear physical interpretation, which can be used to guarantee that a trajectory is feasible for the vehicle by altering the bounds w_b and \tilde{v}_b .

C. Objective Function Formulation

To formulate the planning task as a numerical optimization problem, we define the objective function as follows. First, we drive a simulated vehicle model with the previously trained controller along a trajectory candidate. The simulation is performed in discrete time, i.e. $x_{k+1} = f_{\text{sim}}(x_k)$,

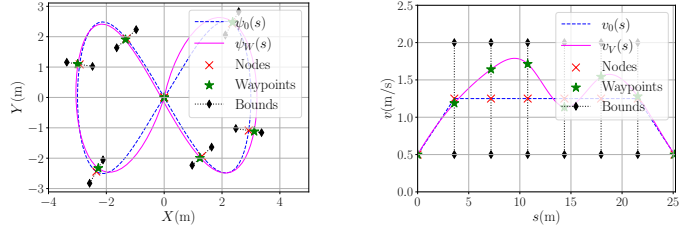


Fig. 3. Waypoint-based parameterization of the reference trajectories: the 2D path (left) and the speed profile (right).

where f_{sim} is the nominal nonlinear vehicle dynamics (15), discretized by 4th order Runge-Kutta algorithm. During the simulation at each time instant k , we observe the GP inputs $z_k = [0_{3 \times 3} \ I_{3 \times 3}]x_k$ and evaluate the variances of the \mathcal{GP}_{1o} and \mathcal{GP}_{1a} , given by (5b). These variances are denoted as $\hat{\Sigma}_{1o}(z_k, X_k)$, $\hat{\Sigma}_{1a}(z_k, X_k)$ to highlight that the variance at k only depends on the current input z_k and the inputs of the training dataset X_k . After the evaluation, we accumulate the variances into a single variable, defined as

$$J_{\mathcal{GP}} = \sum_{k=0}^{N_{\text{sim}}} (\hat{\Sigma}_{1o}(z_k, X_k) + \hat{\Sigma}_{1a}(z_k, X_k)) \quad (27)$$

Finally, we extend the datasets of the GPs by adding z_k at each timestep, i.e. $X_k = X_{k-1} \cup z_k$, while X_0 is the original input dataset. This approach allows us to formulate an objective function that (a) enforces the vehicle to explore the regions where the GP uncertainty is high, (b) accounts for already explored regions, as the addition of new data points reduces the predictive variance in the neighboring regions of z_k .

Note that the simulation is only used during the design as the substitute for the real dynamics. After a trajectory has been obtained, the trajectory will be tracked with the real vehicle for the data collection.

D. Bayesian Optimization

Using the outlined trajectory parameterization and the objective function we can formulate the following optimization for the experiment design:

$$\max_{V, W} J_{\mathcal{GP}} \quad (28a)$$

$$\text{s.t. } V \in [v_{\min}, v_{\max}], \quad (28b)$$

$$W \in [-w_b/2, w_b/2], \quad (28c)$$

$$x_{k+1} = f_{\text{sim}}(x_k), \quad (28d)$$

However, simulating the motion of the vehicle along a given reference and evaluating GPs while simultaneously extending their datasets is computationally demanding, therefore, the number of objective function evaluations is limited. Furthermore, as the derivative of the $J_{\mathcal{GP}}$ cannot be analytically computed and the numerical approximation is difficult, gradient-based optimization methods cannot be used. Therefore, to solve (28), we utilize Bayesian optimization [31] which is a global optimization technique that is suitable for solving problems with computationally expensive cost functions.

After solving (28) the synthesized reference is applied on the vehicle to obtain the new training dataset. Then, (28) can

be solved again with the expanded dataset, achieving dynamic active learning.

VI. \mathcal{L}_2 -GAIN ANALYSIS

In this section, we will analyze the worst-case performance of our entire tool chain for various parameter realizations of the to-be-controlled vehicle. Specifically, we will characterize the induced \mathcal{L}_2 gain of the closed-loop system formed by the nonlinear vehicle model (15) for a given parameter realization and the GP-based controller ((22) and (23)) that was adapted by the same *learning strategy* for each instance of vehicle dynamics. By learning strategy, we mean all the components needed to reproduce the learning process, i.e., the active learning method, the training algorithms, and all initial and tuning parameters. For this purpose, an efficient numerical method is proposed to calculate the closed-loop-induced \mathcal{L}_2 gain from reference to tracking error. This quantitative measure is used to analyze the performance and efficiency of the proposed learning strategy under variations of the vehicle dynamics.

Formally, we consider the closed-loop model in the following form:

$$\mathcal{S} \begin{cases} \dot{x} = f_{\text{cl}}(x, w, \xi) \\ z = h(x, w) \end{cases} \quad (29)$$

where $f_{\text{cl}} : \mathcal{X} \times \mathcal{W} \times \Xi \rightarrow \mathcal{X}$ corresponds to the true vehicle dynamics (15) with (12d)-(12f) and (14) interconnected with the lateral and longitudinal controllers (23) and trained GP-based compensators (22). The argument ξ describes the vector of uncertain model parameters, such as drivetrain parameters, cornering stiffnesses, vehicle mass and inertia parameters that describe different realizations of the true vehicle and are assumed to be bounded in a closed set $\Xi \subset \mathbb{R}^{n_\xi}$. The nominal model is represented by the parameter vector ξ_0 in this set, for which the lateral and longitudinal controllers (23) are designed based on (24) with weighting matrices Q_{1o} , Q_{1a} , R_{1o} , R_{1a} . When $\xi = \xi_0$, then from the adaptation point of view model there is no mismatch, so there is actually no need for GP augmentation and adaptive controller.

To shift the equilibrium to the origin, the longitudinal velocity v_ξ and velocity reference v^r are centered: let $\tilde{v}_\xi = v_\xi - v_{\text{cent}}^r$ and $\tilde{v}^r = v^r - v_{\text{cent}}^r$, where $v_{\text{cent}}^r = (v_{\text{max}}^r + v_{\text{min}}^r)/2$. With these new variables $x = [q \ e_s \ \theta_e \ \tilde{v}_\xi \ v_\eta \ \omega]^\top \in \mathcal{X}$ is the state vector, $w = [\tilde{v}^r \ c]^\top \in \mathcal{W}$ is the generalized disturbance signal and z is the generalized performance signal that contains the tracking errors as $z = h(x, w) = [\tilde{v}_\xi - \tilde{v}^r \ e_s]^\top \in \mathcal{Z}$. Furthermore, to indicate that \tilde{v}^r is only active in the low-frequency range, we augment the system with a first-order, strictly proper, low-pass filter. As a result, the state space is extended by one extra dimension, corresponding to the state of the filter i.e. $\tilde{x} = [q \ e_s \ \theta_e \ v_\eta \ \tilde{v}_\xi \ \omega \ \tilde{v}_f^r]^\top \in \tilde{\mathcal{X}}$. As the filter is strictly proper, the direct feed-through is eliminated from the output equation, i.e., $z = h(\tilde{x}) = [\tilde{v}_\xi - \tilde{v}_f^r \ e_s]^\top$.

For choice of $\xi \in \Xi$, as a first step, an initial sparse GP model is fitted, via the VFE method to obtain the hyperparameters and M inducing points, using a data set with N samples obtained from the nonlinear vehicle model represented by ξ under an input signal u that is fixed among all trials. Then, N_{act} iterations of dynamic active learning in terms of

experiment design and batch-wise adaptation of the sparse GP are accomplished according to Secs. II-C and V with the hyperparameters fixed among trials. This results in a learned compensator (22) that is added to the nominal control law to form the adapted closed-loop system.

The calculation of the \mathcal{L}_2 -gain of the resulting closed loop relies on the theory of dissipative dynamical systems [32]. For a given ξ , system (29) is said to be dissipative w.r.t. a quadratic supply $s(w, z) = \gamma^2 w^\top w - z^\top z$ if there exists a non-negative storage function $V : \tilde{\mathcal{X}} \rightarrow \mathbb{R}^+$ such that, in case V is differentiable, the differential dissipation inequality

$$\dot{V}(\tilde{x}) \leq \gamma^2 w^\top w - z^\top z \quad (30)$$

is satisfied for all (\tilde{x}, z, w) trajectories of \mathcal{S} . If w is restricted to squared integrable signals, i.e. \mathcal{L}_2 , then the induced \mathcal{L}_2 -gain is the smallest γ for which (30) holds, formally: $\sup_{w \in \mathcal{L}_2} \{\|z\|_2 / \|w\|_2\} \leq \gamma$. Furthermore, a finite \mathcal{L}_2 gain also proves asymptotic stability of the corresponding system (w.r.t. a chosen equilibrium point) as V acts as a Lyapunov function if (30) holds strictly [32]. Following this concept, our goal is to find a storage function V and γ . However, constructing V and γ that give a close upper bound on the true gain is difficult for a general nonlinear system.

To overcome this difficulty, we propose an iterative, optimization-based approach, inspired by [33], which consists of two components: a learner and a verifier. First, the learner is responsible for finding a storage function candidate V and corresponding \mathcal{L}_2 -gain γ by solving a convex optimization problem. To formulate the learner, we restrict ourselves to function candidates in the form of $V(x) = \tilde{x}^\top P(\tilde{x})\tilde{x}$, where $P(\tilde{x}) = P_0 + P_1\tilde{x}_1 + \dots + P_7\tilde{x}_7 \succ 0$ as this function class remains linear in the parameters P_i^7 , but is more flexible than the generic quadratic forms.

By substituting the storage function and (29) into (30):

$$J(\tilde{x}, w, \bar{\xi}, \{P_i\}_{i=1}^7, \gamma^2) := \tilde{x}^\top P(\tilde{x})f_{\text{cl}}(\cdot) + f_{\text{cl}}^\top(\cdot)P(\tilde{x})\tilde{x} + \tilde{x}^\top \frac{dP(\tilde{x})}{dt} \tilde{x} - \gamma^2 w^\top w + h^\top(\tilde{x})h(\tilde{x}) \leq 0, \quad (31)$$

where $f_{\text{cl}}(\cdot) = f_{\text{cl}}(\tilde{x}, w, \bar{\xi})$. Note that if \tilde{x} , w are fixed at constant values, (31) is linear in the unknown variables P_i and γ^2 . Therefore, by introducing the finite sets $\mathbb{X} \subset \tilde{\mathcal{X}}$ and $\mathbb{W} \subset \mathcal{W}$, we propose the following convex optimization problem:

$$\min_{P_0, \dots, P_7, \gamma^2} \gamma^2 \quad (32a)$$

$$\text{s.t. } P(\tilde{x}) \succ 0, \quad (32b)$$

$$J(\tilde{x}, w, \xi, \{P_i\}_{i=1}^7, \gamma^2) \leq 0, \quad (32c)$$

$$\forall (\tilde{x}, w) \in \mathbb{X} \times \mathbb{W},$$

where \mathbb{X} and \mathbb{W} are discrete grids, constructed by sampling the compact sets such that the sample points sufficiently cover $\tilde{\mathcal{X}} \times \mathcal{W}$. As (32c) is linear in the optimization variables, we can utilize this gridding approach even up to the case of 6 dimensions, as state-of-the-art numerical solvers can efficiently handle even a large number of linear constraints.

Note that the learner only guarantees that the differential dissipation inequality is satisfied at the discrete grid points. Therefore, a verifier is introduced, which essentially tries to

find counterexamples where (32c) does not hold in $\tilde{\mathcal{X}} \times \mathcal{W}$ for the previously obtained γ^2 and V . For fixed P_i and γ^2 , the verifier is formulated as the nonlinear optimization:

$$\max_{\tilde{x} \in \tilde{\mathcal{X}}, w \in \mathcal{W}} J(\tilde{x}, w, \bar{\xi}, \{P_i\}_{i=1}^7, \gamma^2). \quad (33)$$

As (33) is a small dimensional problem, numerical solvers with efficient algorithmic differentiation (e.g. CasADi [34] - IPOPT [35]) are capable of handling it. Note also that since (35) is nonlinear, there is no guarantee of finding the global optimum. To avoid getting stuck at a local maximum, the optimization can be performed multiple times starting from different initial values. For more sophisticated solutions that can provide mathematical guarantees to cover the entire search space, we can combine this simple heuristic approach with scenario method [36], or use adaptive sampling similar to that proposed in [37]. After solving (33), if J is positive, the corresponding \tilde{x} and w values are added to the discrete sets \mathbb{X} , \mathbb{W} and the iteration is repeated until either (32) becomes infeasible which means that we cannot obtain a bound for the induced \mathcal{L}_2 -gain with the proposed storage function structure or the optimal value of J remains negative which means that an upper bound for \mathcal{L}_2 -gain is found with the storage function V , also showing stability.

With the proposed approach, we obtain the closed-loop \mathcal{L}_2 gain only for a specific vehicle model described by ξ . If we define a sufficiently fine grid $\Xi_g \subset \Xi$, fix a learning strategy, apply it to all vehicle models $\xi \in \Xi_g$ and then perform the \mathcal{L}_2 gain analysis on each resulting closed-loop system, we can obtain quantitative information on the performance of the controllers achievable under different uncertainty realizations.

VII. SIMULATION STUDY

A. Setup and Simulation Environment

The performance of the proposed control architecture is first analyzed in a simulation environment. For the simulation study, we have developed a digital-twin model F1TENTH cars, corresponding to the dynamics discussed in Sec. III-B, using MuJoCo [38], a high-fidelity physics engine, which allows us to reliably test the adaptive schemes, as physical parameters can be easily altered. The nominal model corresponds to a parameter configuration of the MuJoCo model, where the parameters were obtained by identifying a real F1TENTH car, see [24]. The simulation environment and the model parameters are available on GitHub².

To evaluate the performance of the adaptive controller approach, we artificially generated a large model mismatch in the digital-twin. The friction coefficients (f_{wheel}) between the wheels and the ground have been reduced, while their radius (r_{wheel}) and the overall inertia of the vehicle have been increased. The original and altered model parameters are displayed in Tab I. Furthermore, the steering dynamics have also been altered by scaling and adding an offset to it:

$$\hat{\delta} = c_1 \delta + c_0 \quad (34)$$

where $\hat{\delta}$ is the steering input acting on the vehicle, δ is computed by the controller, while c_1 and c_0 are parameters.

TABLE I
INITIAL AND ALTERED MODEL PARAMETERS

	f_{wheel}	I_z (kgm ²)	r_{wheel} (m)	c_1	c_0 (rad)
Initial	2.5	0.078	0.052	1	0
Altered	0.5	0.090	0.072	0.85	0.15

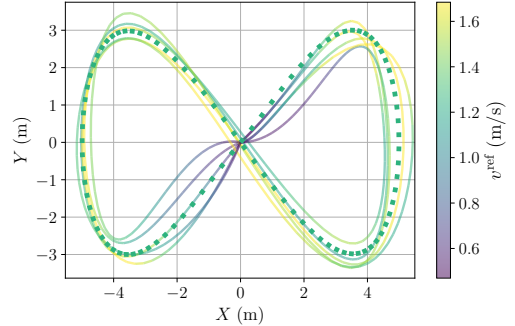


Fig. 4. Initial training trajectory (dashed) and the trajectories obtained by the dynamic active learning (solid)

For the synthesis of the nominal control laws (23) using the baseline single track model, the parameter-dependent gain matrices are obtained by solving (24), which has been implemented in Python with CVXPY [39] and solved with Mosek³. The weighting matrices of the LQR have been tuned using numerical simulations with the model resulting in $Q_{1a} = \text{diag}(1, 80, 0)$, $R_{1a} = 500$ and $Q_{1o} = 1$, $R_{1o} = 100$ for the lateral and longitudinal controller, respectively. Furthermore, the gain of the virtual velocity reference generator is $k_v = 0.1$.

B. Data Collection and GP Training

For initial GP training, we used lemniscate trajectories (Fig. 4) with constant speeds (0.75-1.25-2 m/s) and 25 Hz sampling, resulting in a dataset of $N = 12000$ points. The initial training of the hyperparameters of the GPs has been performed offline by maximizing the VFE cost (8) by gradient descent with $M = 30$. Next, we used the dynamic active learning method from Sec. V to refine the GP components. The algorithm used a lemniscate initial trajectory and a 1.25 m/s constant speed profile were used, with $w_b = 0.5$, $v_{\min} = 0.5$ m/s, and $v_{\max} = 2$ m/s as bounds. We have used $n = 7$ equidistant nodes along the path, yielding 14 optimization variables. variables were optimized using 25 initial samples and 20 iterations per trajectory synthesis. The optimization has been performed using 25 initial samples and a total of 20 iterations. The trajectories are shown in Fig. 4.

Using the data collected along the trajectories, we retrained the GP components in a batch-wise manner with the augmented datasets. We performed 5 iterations of the dynamic active learning, where during each iteration, we collected additional training data along a new trajectory and retrained the GPs. At each iteration, for the sake of the analysis, we evaluated the cumulative variance (27) along a separate test trajectory to quantify how the active learning method improves the uncertainty of the approximation. As the results show in Fig. 5, the proposed dynamic active learning efficiently reduced the cumulative variance after each iteration.

²<https://github.com/AIMotionLab-SZTAKI/AiMotionlab-Virtual>

³<https://www.mosek.com>

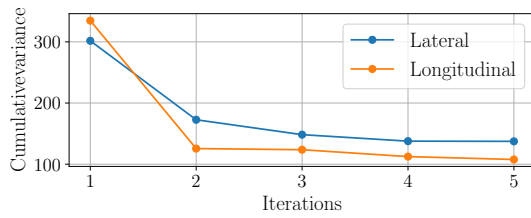


Fig. 5. Cumulative variance of the GPs after each iteration of the dynamic active learning algorithm.

TABLE II
TRACKING ERRORS OF THE NOMINAL, THE RLS-BASED (RLS-GP) AND THE RGB-BASED (RGB-GP) ONLINE ADAPTIVE CONTROLLERS.

	$\max(e_s)$	$\max(s_{err})$	$\ e_s\ _{RMS}$	$\ s_{err}\ _{RMS}$
LPV-LQ	0.12	1.16	0.07	0.83
RLS-GP	0.05	0.37	0.01	0.15
RBG-GP	0.04	0.28	0.01	0.14

C. Adaptive Control

To demonstrate the efficiency of the proposed control algorithm, we compare three scenarios, where the vehicle tracks the same predefined trajectory. In the first scenario (LPV-LQ), only the nominal feedback laws (23) are used. Then, in the second and third scenarios, we utilize the GP-based adaptive compensator (22) along with the nominal controller. For online adaptation of the GPs, we start from the offline estimated GP and apply the RLS-GP method of [11] and the RGB-GP method of Sec. II-C with $Z = 20$ batch size. Furthermore, for the RLS-GP $\gamma = 0.995$ forgetting factor and $\beta = 0.9$ confidence level has been used, while for the RGB-GP $n_\alpha = 5$ update iteration has been selected to maintain computational feasibility, with $\alpha = 0.1$ learning rate.

The simulation results are depicted in Fig. 6. As shown, due to the significant model mismatch, the nominal controller cannot track the reference accurately, as both the lateral (e_s), and the heading (θ_e) errors are significant. Furthermore, a steady-state error occurs in the longitudinal velocity (v_{err}) that results in increased longitudinal position error (s_{err}). On the other hand, we can observe that the adaptive controllers can efficiently decrease the tracking errors and ensure the precise tracking of the reference trajectories. A comparison between the control inputs generated by the LPV-LQ and the two GP-based adaptive algorithms is also displayed. Finally, to quantify the tracking performance, the maximum and *root mean square* (RMS) values of the tracking errors are collected in Tab. II. As the table and the figure show, the RBG-GP provides less noisy estimates and superior tracking performance compared to the RLS-GP.

D. Performance Verification by \mathcal{L}_2 Gain Analysis

We provide performance analysis of the *learning strategy* of Sec. VII-B and the adaptive control scheme of Sec. VII-C using the algorithm proposed in Sec. VI. For the analysis, we consider the nonlinear closed-loop with the uncertain parameters $\xi = [C_r \ C_f \ C_{m1} \ C_{m2} \ C_{m3} \ I_z]$ as these are the values that are generally harder to identify and can vary based on changing environmental condition. Furthermore, the Ξ set is defined such that each parameter has a maximum 30% mismatch. We specified the discrete grid $\Xi_g \in \Xi$ by sampling

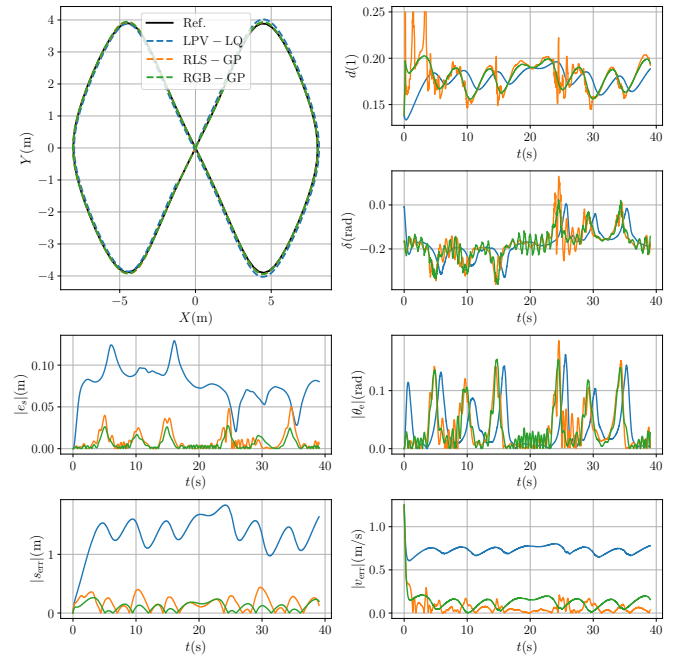


Fig. 6. Comparison of the simulation results using the nominal and adaptive tracking controllers.

4 points equidistantly along each dimension, yielding 4096 realizations. For each realization, the \mathcal{L}_2 -gain computation is implemented in Python, where the learner (32) is formulated in CVXPY and solved with Mosek, while the verifier is handled by CasADi and IPOPT. As discussed in Sec. VI, a low-pass filter with 10 Hz cutoff is used for shaping the reference which is defined in the range $v^r \in [0.5, 2]$ m/s. The region of interest⁴ for \mathcal{X} and \mathcal{W} are obtained from simulation results and are discretized with an initial equidistant grid of 5 points along each dimension. In all the cases, the algorithm converged with iteration numbers between 89 and 278. The resulting upper bounds on the induced \mathcal{L}_2 took values in the range $\mathcal{L}_2 \in [0.084, 0.101]$. Furthermore, we computed the induced \mathcal{L}_2 -gain of the nominal closed-loop system, resulting in $\mathcal{L}_2 = 0.104$. Note that GP augmentation supersedes this, as during the nominal control design, we employed simplifications. From the results, we can conclude that the proposed *learning strategy* can efficiently compensate for the introduced model mismatch under all plant variations, and can restore the original performance.

Note that the altered digital-twin model we considered in the previous subsections corresponds to the parameter vector $\xi_{MJ} = [35.12, 23.36, 37.98, 2.26, 0.79, 0.09]$, which is in Ξ . Hence, our analysis also explains the observed impressive control performance and we can characterize the magnitude of variation of the vehicle dynamics for which we can expect good performance of the learning approach, i.e., when it is safe to deploy the method, which represents the true practical value of the discussed analysis approach.

$$\begin{aligned}
 {}^4\mathcal{X} &:= [-0.2, 0.2] \times [-0.2, 0.2] \times [-0.5, 0.5] \times \\
 &[-0.5, 0.5] \times [-0.75, 0.75] \times [-3.5, 3.5] \times [-0.75, 0.75], \\
 \mathcal{W} &:= [-1.44, 1.44, -0.75, 0.75]
 \end{aligned}$$

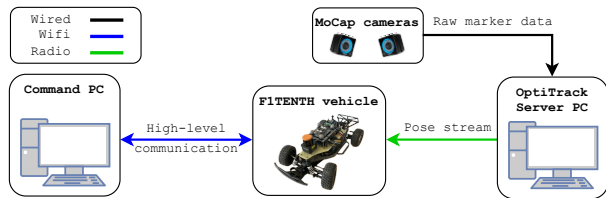


Fig. 7. Communication architecture of the test environment.

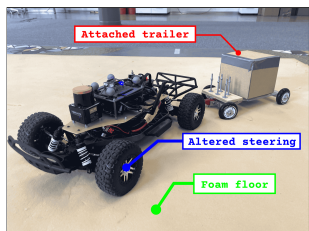


Fig. 8. Modifications made on the FITENTH platform to artificially generate model mismatch.

VIII. IMPLEMENTATION AND EXPERIMENTAL STUDY

A. Test Environment

The experiments are performed using the previously introduced FITENTH [20] vehicles. For indoor positioning, an OptiTrack motion-capture system is utilized that provides submillimeter position and orientation data. The positioning system and the vehicles are interconnected via Crazyradio PA dongles, which enable low-latency point-to-point communication. The high-level commands and experiment management are achieved through TCP protocol via WiFi. The overall architecture is depicted in Fig. 7. The main computation unit of the vehicle is an Nvidia Jetson Orin Nano that runs the control algorithm at 60 Hz, implemented in a ROS2-based onboard software stack available at GitHub⁵.

B. Experimental Results

The trajectory-tracking performance of the proposed adaptive control method has been evaluated similarly to the simulation studies. First, we generated a significant model mismatch between the previously identified (nominal) model and the real vehicle. As shown in Fig. 8, a trailer with $m = 2.5$ kg weight is attached to the car. To modify the wheel-ground contact, we used foam instead of the regular carpet of the lab. Furthermore, we modified the steering dynamics by introducing the offset and gain characteristics (34).

Next, we capture the model mismatch by training the GP components offline. We utilized the lemniscate trajectories of Fig. 4 for data collection with constant reference velocities 0.75, 1.25, and 2 m/s as this learning strategy has been validated in simulations. The resulting dataset contained $N = 6000$ training points obtained with 25 Hz sampling frequency. To further increase the informative training data, we collected additional samples by executing one iteration of the active-learning-based experiment design. One iteration could sufficiently refine the GPs based on Fig. 5. For the training, we utilized the SGP regression outlined in Sec. II-B with $M = 30$

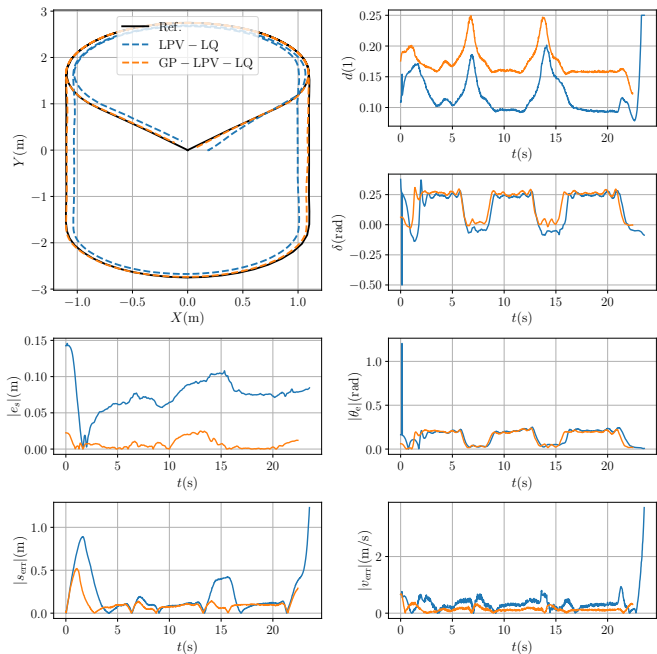


Fig. 9. Experimental results of the proposed control scheme.

inducing points for both the lateral and the longitudinal subsystems, respectively, similarly to the simulation study. The training of the GP components is carried out with GPyTorch. During the experiments, continuous time state-feedback (22)-(23) is evaluated at 60 Hz, which is feasible on embedded hardware, as only 30 inducing points are used by the GP components, keeping the control cycle time under 0.01 s.

After the hyperparameters of the GPs had been trained, we analyzed the performance of the controller in an experiment. The measurement results are displayed in Fig. 9, where the nominal LPV-LQ (without the GP-based adaptive terms) and the adaptive GP-LPV-LQ are compared. As shown, although, the LPV-LQ has been able to execute the prescribed trajectory, the tracking performance significantly decreased compared to the nominal case and the adaptive controllers, due to the noticeable model mismatch introduced in both the lateral and the longitudinal subsystems.

As the orange lines show, the learning components of the adaptive GP-LPV-LQ have successfully captured the model mismatch and the controller has been able to compensate. A comparison of the maximal and RMS values is presented in Tab. III. It is clear that by using the proposed adaptive trajectory-tracking controller, the vehicle has been able to precisely track the reference. However, in both experiments, an initial temporary increase in the longitudinal position error can be observed. Although the GP-based adaptive compensator has reduced the magnitude of the error, it is not negligible. The primary reason for this is that the wheels of the vehicle sink into the soft foam floor, creating an initial sticking effect that the controller needs to overcome. Additionally, a small delay between the prescribed reference and the launch of the control algorithm may contribute to the initial surge in longitudinal error. Nevertheless, it is notable that after 5 seconds, the controller recovered and the performance became satisfactory.

⁵<https://github.com/AIMotionLab-SZTAKI/AIMotionLab-FITENTH>

TABLE III

TRACKING ERRORS CORRESPONDING TO THE EXPERIMENTS PERFORMED WITH THE FITENTH VEHICLE.

	$\max(e_s)$	$\max(s_{err})$	$\ e_s\ _{RMS}$	$\ s_{err}\ _{RMS}$
LPV-LQ	0.11	0.89	0.08	0.29
GP-LPV-LQ	0.02	0.53	0.01	0.13

IX. CONCLUSION

In this article, a learning-based adaptive control method has been proposed for autonomous ground vehicles to ensure reliable trajectory tracking in the presence of modeling uncertainties. By decoupling the nonlinear vehicle dynamics, augmenting the subsystems with sparse GPs and developing efficient active-learning and recursive sparse GP training methods, we have been able to efficiently capture and compensate for up to 30% of model mismatch w.r.t. a nominal first principle model. The proposed control method has been successfully tested on both a high-fidelity simulator and a real vehicle, demonstrating its practical applicability. To analyze the proposed learning strategy and control architecture, we have developed a counterexample-based algorithm to estimate the induced \mathcal{L}_2 -gain of the closed-loop system.

REFERENCES

- [1] J. Betz, H. Zheng, A. Liniger, U. Rosolia, P. Karle, M. Behl, V. Krovi, and R. Mangharam, "Autonomous vehicles on the edge: A survey on autonomous vehicle racing," *IEEE Open J. Intell. Trans. Sys.*, vol. 3, pp. 458–488, 2022.
- [2] B. Balaji, S. Malloya, S. Genc, S. Gupta, L. Dirac, V. Khare, G. Roy, T. Sun, Y. Tao, B. Townsend, E. Calleja, S. Muralidhara, and D. Karuppusamy, "Deepracer: Educational autonomous racing platform for experimentation with sim2real reinforcement learning," *arXiv preprint:1911.01562*, 2019.
- [3] U. Rosolia, A. Carvalho, and F. Borrelli, "Autonomous racing using learning model predictive control," in *Proc. Amer. Control Conf.*, 2017, pp. 5115–5120.
- [4] A. Liniger, A. Domahidi, and M. Morari, "Optimization-based autonomous racing of 1:43 scale rc cars," *Opt. Control Appl. Meth.*, vol. 36, no. 5, p. 628–647, 2015.
- [5] J. Becker, N. Imholz, L. Schwarzenbach, E. Ghignone, N. Baumann, and M. Magno, "Model- and acceleration-based pursuit controller for high-performance autonomous racing," in *Proc. IEEE Int. Conf. Rob. Aut.*, 2023, pp. 5276–5283.
- [6] S. Vaskov, R. Quirynen, M. Menner, and K. Berntorp, "Friction-adaptive stochastic predictive control for trajectory tracking of autonomous vehicles," in *Proc. Amer. Control Conf.*, 2022, pp. 1970–1975.
- [7] Y. Kebbaty, V. Puig, N. Ait-Oufroukh, V. Vigneron, and D. Ichalal, "Optimized adaptive mpc for lateral control of autonomous vehicles," in *Proc. 9th Int. Conf. Control, Mechat. Auto.*, 2021, pp. 95–103.
- [8] X. Ji, X. He, C. Lv, Y. Liu, and J. Wu, "Adaptive-neural-network-based robust lateral motion control for autonomous vehicle at driving limits," *Control Eng. Prac.*, vol. 76, pp. 41–53, 2018.
- [9] J. Kabzan, L. Hewing, A. Liniger, and M. N. Zeilinger, "Learning-based model predictive control for autonomous racing," *IEEE Rob. Aut. Let.*, vol. 4, no. 4, pp. 3363–3370, 2019.
- [10] L. Hewing, J. Kabzan, and M. N. Zeilinger, "Cautious model predictive control using gaussian process regression," *IEEE Trans. Control Sys. Tech.*, vol. 28, no. 6, pp. 2736–2743, 2020.
- [11] Y. Liu, P. Wang, and R. Tóth, "Learning for predictive control: A dual gaussian process approach," *arXiv preprint: 2211.03699*, 2022.
- [12] A. Carron, E. Arcari, M. Wermelinger, L. Hewing, M. Hutter, and M. N. Zeilinger, "Data-driven model predictive control for trajectory tracking with a robotic arm," *IEEE Rob. Aut. Let.*, vol. 4, no. 4, pp. 3758–3765, 2019.
- [13] M. Kiss, R. Tóth, and M. Schoukens, "Space-filling input design for nonlinear state-space identification," 2024.
- [14] A. Krause, A. Singh, and C. Guestrin, "Near-optimal sensor placements in gaussian processes: Theory, efficient algorithms and empirical studies," *J. Mach. Learn. Res.*, 2008.
- [15] D. Gángó, T. Péni, and R. Tóth, "Learning based approximate model predictive control for nonlinear systems," *IFAC-PapersOnLine*, vol. 52, no. 28, pp. 152–157, 2019.
- [16] G. Gagliardi, V. D'Angelo, and A. Casavola, "Combined longitudinal and lateral dynamics regulation of autonomous vehicles via induced \mathcal{L}_2 -gain linear parameter varying control strategies based on parameter-dependent lyapunov functions," *International Journal of Robust and Nonlinear Control*, vol. 34, 03 2024.
- [17] A. Gupta, M. Nilsson, P. Falcone, E. Klintberg, and L. J. Mårdh, "A framework for vehicle lateral motion control with guaranteed tracking and performance," in *Proc. IEEE Intell. Trans. Sys. Conf.*, 2019, pp. 3607–3612.
- [18] B. Paden, M. Čáp, S. Z. Yong, D. Yershov, and E. Frazzoli, "A survey of motion planning and control techniques for self-driving urban vehicles," *IEEE Trans. Intell. Veh.*, vol. 1, no. 1, pp. 33–55, 2016.
- [19] K. Floch, T. Péni, and R. Tóth, "Gaussian-process-based adaptive trajectory tracking control for autonomous ground vehicles," in *Proc. Eur. Control Conf.*, 2024.
- [20] M. O'Kelly, H. Zheng, D. Karthik, and R. Mangharam, "F1tenth: An open-source evaluation environment for continuous control and reinforcement learning," in *Proc. NeurIPS*, ser. Proc. Machine Learn. Res., vol. 123. PMLR, 12 2020, pp. 77–89.
- [21] C. E. Rasmussen and C. K. I. Williams, *Gaussian Processes for Machine Learning*. The MIT Press, 2006.
- [22] P. Antal, T. Péni, and R. Tóth, "Backflipping with miniature quadcopters by gaussian-process-based control and planning," *IEEE Trans. Control Sys. Tech.*, pp. 1–12, 2023.
- [23] M. Titsias, "Variational learning of inducing variables in sparse gaussian processes," in *Proc. 12th Int. Conf. Artif. Intell. Stat.*, vol. 5. PMLR, 04 2009, pp. 567–574.
- [24] K. Floch, "Model-based motion control of the f1tenth autonomous electrical vehicle," Bachelor's thesis, Budapest University of Technology and Economics, 2022.
- [25] R. Tóth, *Modeling and Identification of Linear Parameter-Varying Systems*. Springer Berlin, Heidelberg, 2010.
- [26] C. Hu, R. Wang, F. Yan, and N. Chen, "Should the desired heading in path following of autonomous vehicles be the tangent direction of the desired path?" *IEEE Trans. Intell. Trans. Sys.*, vol. 16, no. 6, pp. 3084–3094, 2015.
- [27] G. M. Hoffmann, C. J. Tomlin, M. Montemerlo, and S. Thrun, "Autonomous automobile trajectory tracking for off-road driving: Controller design, experimental validation and racing," in *Proc. Amer. Control Conf.*, 2007, pp. 2296–2301.
- [28] V. Laurain, R. Tóth, D. Piga, and W. X. Zheng, "An instrumental least squares support vector machine for nonlinear system identification," *Automatica*, vol. 54, pp. 340–347, 2015.
- [29] F. Wu, "Control of linear parameter varying systems," Ph.D. dissertation, University of California at Berkeley, 1995.
- [30] A. Jain and M. Morari, "Computing the racing line using Bayesian optimization," in *Proc. 59th IEEE Conf. on Decis. Control*, 2020.
- [31] P. I. Frazier, "A tutorial on bayesian optimization," *arXiv: 1807.02811*, 2018.
- [32] A. van der Schaft, *\mathcal{L}_2 -Gain and Passivity Techniques in Nonlinear Control*. Springer Cham, 2017.
- [33] S. Chen, M. Fazlyab, M. Morari, G. J. Pappas, and V. M. Preciado, "Learning lyapunov functions for hybrid systems," in *Proc. 24th Int. Conf. Hybrid Sys.: Computation and Control*, 2021.
- [34] J. A. E. Andersson, J. Gillis, G. Horn, J. B. Rawlings, and M. Diehl, "CasADi – A software framework for nonlinear optimization and optimal control," *Math. Prog. Comp.*, vol. 11, no. 1, pp. 1–36, 2019.
- [35] A. Wächter and L. Biegler, "On the implementation of an interior-point filter line-search algorithm for large-scale nonlinear programming," *Math. Prog.*, vol. 106, pp. 25–57, 03 2006.
- [36] M. C. Campi, S. Garatti, and F. A. Ramponi, "A general scenario theory for nonconvex optimization and decision making," *IEEE Trans. Autom. Control*, vol. 63, no. 12, p. 4067–4078, 2018.
- [37] R. Bobiti and M. Lazar, "Automated-sampling-based stability verification and doa estimation for nonlinear systems," *IEEE Trans. Autom. Control*, vol. 63, no. 11, p. 3659–3674, 2018.
- [38] E. Todorov, T. Erez, and Y. Tassa, "Mujoco: A physics engine for model-based control," in *Proc. IEEE/RSJ Int. Conf. Intell. Rob. Sys.*, 2012, pp. 5026–5033.
- [39] S. Diamond and S. Boyd, "CVXPY: A Python-embedded modeling language for convex optimization," *J. Mach. Learn. Res.*, vol. 17, no. 83, pp. 1–5, 2016.